Molecular Catalysis 582 (2025) 115179

Contents lists available at ScienceDirect

Molecular Catalysis

journal homepage: www.journals.elsevier.com/molecular-catalysis

Research Paper

A combined DFT-Experimental study on FSP-made Ru/Ti-SiO_2 catalysts for CO_2 methanation

Okorn Mekasuwandumrong [a,1], Tinnakorn Saelee [b,c,1], Jakapob Noppakhun [d,e,f], Meena Rittiruam [b,c], Patcharaporn Khajondetchairit [g], Damien P. Debecker [h], Supareak Praserthdam [d,e,f,*], Piyasan Praserthdam [b,c]

[a] Department of Chemical Engineering, Faculty of Engineering and Industrial Technology, Silpakorn University, Nakorn Pathom 73000, Thailand
[b] Futuristic Science Research Center, School of Science, Walailak University, Nakhon Si Thammarat 80160, Thailand
[c] Research Center for Theoretical Simulation and Applied Research in Bioscience and Sensing, Walailak University, Nakhon Si Thammarat, Thasala 80160, Thailand
[d] Department of Chemical Engineering, Faculty of Engineering, Chulalongkorn University, Bangkok, 10330, Thailand
[e] Center of Excellence on Catalysis and Catalytic Reaction (CECC), Chulalongkorn University, Bangkok, 10330, Thailand
[f] High-performance Computing Unit (CECC-HCU), Chulalongkorn University, Bangkok, 10330, Thailand
[g] KOSEN-KMITL, King Mongkut's Institute of Technology Ladkrabang, Bangkok, 10520, Thailand
[h] Institute of Condensed Matter and Nanosciences (IMCN), Université catholique de Louvain (UCLouvain), Place Louis Pasteur, 1, 1348 Louvain-la-Neuve, Belgium

ARTICLE INFO

Keywords:
CO_2
Methanation
Ru
SiO2
Ti
Flame spray pyrolysis

ABSTRACT

Flame spray pyrolysis (FSP) was employed to synthesize Ti-modified SiO_2 in a single step, serving as the support for Ru-based catalysts in CO_2 methanation reactions. The addition of Ti led to the formation of anatase and rutile TiO_2 phases, enhancing the catalytic activity of Ru/Ti-SiO_2 catalysts. Benchmarking between Ru/Ti-SiO_2 catalysts of various Ti concentrations prepared using one-step FSP techniques indicated significantly higher catalytic activity for the impregnation-made catalysts compared to the FSP-made ones, where diffuse reflectance infrared Fourier transform spectroscopy (DRIFTS) revealed different CH_4 formation mechanisms between two techniques. For FSP-made catalysts, it predominantly occurred through the CO route, whereas the impregnation-made proceed via both the dissociative adsorption of CO_2 (CO route) and through surface formate species formation. To explain the effect of Ti loading on Ru/SiO_2 catalysts, a multiscale analysis combining density functional theory (DFT) and microkinetic modeling was performed to study the adsorption behavior of CO_2 on different catalysts. The results revealed that a high amount of Ti reduced the adsorption strength of CO_2 on Ru/SiO_2 catalysts, indicating a modified interaction between CO_2 and the catalyst surface.

1. Introduction

Environmental pollution has become a global concern since it could affect all living things. Carbon dioxide, released from fossil fuel combustion, is the primary pollutant that can lead to global warming and climate change. Thus, it is necessary to curb net CO_2 emissions into the atmosphere. CO_2 utilization is one of the options focused on converting carbon dioxide into value-added compounds [1]. CO_2 methanation (equation (1)) is the reaction that converts carbon dioxide and hydrogen into methane (and water). It is considered a relevant route to reduce carbon dioxide emissions and convert green electricity surplus into green hydrogen into a chemical fuel (methane) that can easily be stored and distributed [2,3].

$$CO_2 + 4H_2 \rightarrow CH_4 + 2H_2O \ \Delta H_{298K} = -252.9 \text{ kJ/mol} \quad (1)$$

Although there are many benefits of CO_2 hydrogenation to methane – which can be operated under atmospheric pressure – the intrinsic activity of methanation catalysts still needs to be improved [4]; hydrogenation of carbon dioxide to methane can be catalyzed by a group of metals, including Ni, Ru, Rh, Pt, Pd, and Co supported on various supports such as titanium oxides, alumina, silica, cerium oxide and magnesium oxide [5–10]. Ni-based catalysts have been widely investigated due to their low cost, high availability, and low-pressure operating conditions. However, Ni catalysts are known for their moderate activity

* Corresponding author at: Department of Chemical Engineering, Faculty of Engineering, Chulalongkorn University, Bangkok, 10330, Thailand.
E-mail address: supareak.p@chula.ac.th (S. Praserthdam).
[1] These authors contributed equally to this work.

https://doi.org/10.1016/j.mcat.2025.115179
Received 29 October 2024; Received in revised form 21 April 2025; Accepted 29 April 2025
2468-8231/© 2025 Elsevier B.V. All rights are reserved, including those for text and data mining, AI training, and similar technologies.

at low temperatures and the need to operate at higher temperatures, where thermodynamics is less favorable and the formation of CO increases. Moreover, Ni catalysts can undergo deactivation by sintering at relatively low temperatures and carbon deposition [11,12]. Therefore, Ru–based catalysts with high catalytic activity and stability over various operating conditions have great potential [13,14].

Generally, Ru-based catalysts show high CO_2 conversion, methane selectivity, and thermal stability in various operation conditions [15–17]. The catalytic performance in CO_2 methanation of Ru-based catalysts depends on their nanoscale properties, such as Ru nanoparticle size and shape, interactions with the support, and effect of dopants [18–20]. Thus, many efforts are focused on developing advanced preparation techniques that offer good control of those properties.

Flame spray pyrolysis (FSP) is one of the most interesting processes for nanomaterial synthesis because it can produce high-purity nanocrystalline materials in one step at low operating cost and is suitable for the large-scale production of catalytic materials [21,22]. Moreover, this method is very versatile because a wide range of precursors, solvents, and operating conditions can be used. Therefore, it offers ways to control the shape, size, composition, surface composition, and crystalline structure of the obtained particles [23,24]. In previous research, various catalysts with excellent and unique properties have been synthesized using FSP and exploited in many reaction applications, e.g., Au–ZnO and Pt–ZnO catalysts for photocatalytic degradation of dyes, Ni-based catalysts for steam reforming reactions of ethanol and glycerol, and Mo-based catalysts for olefin metathesis [25–27].

In this work, the Ru was either impregnated onto Ti-doped silica materials made by FSP or directly incorporated in the FSP precursors solution to perform a one-step synthesis. The physicochemical properties of the catalysts were characterized via N_2 physisorption (BET), X-ray diffraction (XRD), H_2 chemisorption, and X-ray photoelectron spectroscopy (XPS). The obtained catalysts were tested in a CO_2 methanation reaction, and the reaction mechanism was studied using in-situ diffuse reflectance infrared Fourier transform spectroscopy. The effect of Ti loading on the adsorption behavior of CO_2 on Ru/SiO_2 catalysts was also investigated using a multiscale analysis combining density functional theory (DFT) and microkinetic modeling.

2. Experimental details

2.1. Catalytic preparation

Synthesis of FPS-made Ru supported on Ti-modified SiO_2 (F-Ru-xTi-SiO_2) catalysts and Ti-SiO_2 supports (F-xTi-SiO_2) were carried out using a flame spray pyrolysis reactor. Ruthenium (III) acetylacetonate (Sigma-Aldrich), Tetraethyl orthosilicate (Sigma-Aldrich), and Titanium (IV) butoxide (Sigma-Aldrich) were used as ruthenium, silicon and titanium precursors, respectively. Xylene (Merck) was used as the solvent. The liquid precursor was prepared by dissolving the desired amounts of all precursors in xylene with a total metal concentration of 0.3 M. The precursor solution was fed at 5 mL/min into the flame spray pyrolysis apparatus using a syringe pump and dispersed with 5 L/min of oxygen to form a fine spray aerosol. The pressure drops at the capillary tip were maintained at 1.5 bar by adjusting the orifice gap area at the nozzle. The spray was ignited by a supporting flame fed with methane (1.5 L/min) and oxygen (3 L/min), positioned in a ring around the nozzle outlet. A sintered metal plate ring provided an additional 10 L/min of oxygen as a sheath for the supporting flame. The product particles were produced by passing through the flame in milliseconds and collected on a glass fiber filter with a vacuum pump. In this work, the loading content of Ru was fixed at 2wt%, and the Ti loading contents (x) varied from 2 to 12wt%.

The FSP-made Ti-modified SiO2 supports were impregnated by Ru precursor solution (ruthenium (III) acetylacetonate and xylene) to compare the catalytic activity. The loading content of Ru was 2wt%. The obtained powder was dried at room temperature for 6 h and in the oven at 120 °C for 24 h. The dried samples were calcined at 350 °C for 2 h. The obtained catalysts were labeled as I-Ru/F-xTi-SiO_2, where x is the atomic percent loading of Ti.

2.2. Catalytic characterization

The crystal structures of catalyst particles were examined by powder X-ray diffraction (XRD) technique using SIEMENS XRD D5000 X-ray diffractometer with CuKα radiation. The scanning was recorded over 2θ angles from 10 to 80. The average crystallite size of catalysts was calculated from line broadening according to Scherrer's equation. The BET surface area, total pore volume, and average pore size diameter were derived from the nitrogen adsorption isotherm at 77 K using a BELSORP automated system. H_2-chemisorption was used to determine the Ru active sites of the catalyst samples. The catalyst was pre-reduced in a 25 ml/min H_2 flow at 400 °C for 2 h, with a 10 °C/min heating rate. After that, the catalyst was cooled to room temperature under a helium atmosphere. The Ru active sites were measured with injected pulses of CO until the sample was saturated. The adsorption result was obtained using Micrometritics Chemisorb 2750 and ASAP 2101CV.3.00 software. The surface concentration and chemical state of the elements were measured using X-ray photoelectron spectra (XPS) in an AMICUS electron spectrometer equipped with an Mg Kα X-ray as the primary excitation and using KRATOS VISION II software. DRIFTS?

2.3. Catalytic activity

The activity tests in the CO_2 hydrogenation reaction were performed in a continuous-flow fixed-bed reactor with an inner diameter of 7.1 mm under atmospheric pressure. A catalyst of 0.1 g was loaded in the reactor and then reduced with a 30 ml/min flow of H_2 at 200 °C for 2 hours before the reaction test. The reaction was carried out using a temperature-programmed reaction method from 200 to 400 °C, which increased continuously by 50 °C per hour. The gas mixture between CO_2, H_2, and He with 20 ml/min was fed into the reactor with a molar ratio (CO_2/ H_2/He = 1/4/3.33). The outlet gas composition was analyzed using a pulse inlet for GC-TCD and GC-FID with a molecular sieve and the porapack Q columns.

3. Computational details

All calculations, structural relaxation, and electronic charge analysis were performed based on the spin-polarized density functional theory (DFT) [28], which is implemented on the Vienna ab initio simulation package (VASP Version 5.4.4) [29–32]. The Projected augmented wave (PAW) method [33,34], combined with the generalized gradient approximation (GGA) method developed by Perdew–Burke–Ernzerhof (PBE) [35], was utilized to define the behavior of an electron in the ion core and valence electrons. The partial occupancy for solving the Kohn-Sham equation of Ru(0001) surface is the first-order Methfessel--Paxton scheme [36] with a smearing width of 0.2 eV, whereas the Gaussian smearing with the smearing width of 0.05 was applied for other metal oxide surfaces. Moreover, the cutoff energy for all systems is set at 400 eV during the structural optimization. The Brillouin zone [37] was defined by the k-point mesh of $3 \times 5 \times 1$ and $3 \times 3 \times 1$ for Ru(0001) and other oxide surfaces, respectively. Structural relaxation was achieved when the energy and force convergence criteria were $<10^{-5}$ eV and 0.05 eV/Å, respectively. For the anatase TiO_2 (A-TiO_2), The Hubbard-*U* correction of 8.5 eV and 9.5 eV [38,39] were used to explain the band gap of oxide materials correctly[40–45]. Additionally, the Van der Waal interaction was considered using the DFT-D3 proposed by Grimme et al., which was added to explain the non-covalent interaction within the system [46].

The slab model representing the Ru catalyst during the CO_2 methanation reaction is constructed as Ru (0001), where it is modeled as a 4-layer slab cleaved from the optimized bulk Ru with space group of $P6_3/$

mmc [47–55]. For the Ru/P25-TiO_2 catalyst, the anatase TiO_2 and rutile TiO_2 are selected to investigate the catalyst behavior during CO_2 methanation. be the most stable surface of anatase TiO_2 [56–60], and rutile TiO_2 the Ru atom is deposited on the optimized anatase TiO_2.

For the SiO_2, the surface is cleaved as SiO_2 (111) from the ß-cristobalite SiO_2, which is reported to exhibit close density and refractive index to amorphous SiO_2, as found in our experiment [61–66]. The model is a three-layer slab with an H atom at the bottom of the third layer representing the silanol group in SiO_2. For designing the 12 % Ti-doped SiO_2, one atom of Ti is substituted into the top layer of SiO_2, exhibiting eight atoms of SiO_2 to represent the doping of SiO_2 catalyst with 12 %Ti. Finally, a Ru atom is placed on both SiO_2 and 12 %Ti-SiO_2 optimized surface to represent the Ru/SiO_2 and Ru/12 %Ti-SiO_2 catalyst.

4. Results and discussion

4.1. Characterization of Ru/Ti-SiO_2 catalysts

The XRD profiles of all FSP-made catalysts (F-Ru-Ti-SiO_2) are shown in Fig. 1. F-Ru-SiO_2 catalyst exhibited the major broad XRD band structure of the amorphous phase of SiO_2 with additional peaks of RuO_2 phase at 2θ around 27, 36°, and 54 [67]. The addition of Ti dopant resulted in the formation of anatase TiO_2 phase at $2\theta = 25$, 38, 48, and 61 with a minor presence of rutile phase at $2\theta = 27$ [25]. The peak intensity and the crystallite size of the TiO_2 phase increased with increasing Ti contents. The crystallite size of all catalysts is calculated using the Scherrer equation, and the results obtained are summarized in Table 1. Increasing Ti content slightly increased the crystallite size of the anatase TiO_2 phase from ~11 nm to ~15 nm.

The N_2 adsorption-desorption isotherms, BET surface area, and total pore volume were determined by the N_2-physisorption technique. The N_2 adsorption-desorption isotherms and pores size distribution of the FSP-made Ru-supported SiO_2 catalysts before and after doping with Ti are shown in Fig. 2. Both isotherms exhibited the type IV physisorption isotherms with type H3 hysteresis loop starting at high P/P_o, corresponding to the characteristic of macroporous materials with pore diameters larger than 50 nm as seen in Fig. 3. The BET surface area and total pore volume of all catalysts are also summarized in Table 1. The BET surface area and total pore volume of FSP-made catalysts increased from 212 to 253 m^2/g and 0.37 to 0.41 cm^3/g as the Ti loading content increased from 0 to 12wt%, respectively. This was probably due to the insertion of the Ti molecule in the SiO_2 matrix, which retards the growth of dense silica domains. H_2 chemisorption results and the deducted Ru dispersion of all FSP-made catalysts after reduction at 400 °C are also given in Table 1. The increase of Ti content from 0 to 12wt% resulted in an increase in H_2 uptake by chemisorption from 0.91 to 1.4 micromole/g_{cat}, corresponding to an increase in dispersion from 1.8 to 2.7 %.

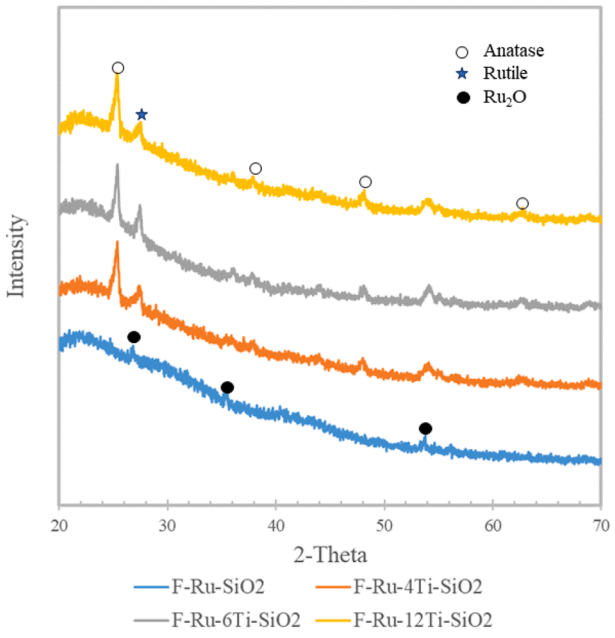


Fig. 1. XRD profiles of all FSP-made Ru/SiO_2 and Ru/Ti-SiO_2 catalysts.

Table 1
The physiochemical of all FSP-made catalysts.

Catalyst	BET surface areas (m^2/g)	Pore Volume (cm^3/g)	d_{XRD} (nm)[a]	Active site (μmol/g-cat)	Dispersion (%)
F-Ru-SiO_2	212	0.37	–	0.91	1.8
F-Ru-4 % Ti-SiO_2	226.8	0.42	11.1	1.03	2
F-Ru-6 % Ti-SiO_2	247.7	0.43	12.3	1.25	2.4
F-Ru-12 % Ti-SiO_2	253.5	0.41	14.5	1.40	2.7

[a] Calculated by using the Scherrer equation from anatase peak at 2θ−25.

The surface compositions and chemical states of FSP-made Ru/SiO_2 and Ru/Ti-SiO_2 catalysts were determined via X-ray photoelectron spectroscopy (XPS), and the XPS spectra of O 1 s, Si 2p, and Ti 2p of FSP-made catalysts are shown in Fig. 3. Typical binding energy of metallic Ru^0 and Ru^{4+} were reported to be 279.5 and 281.4 eV, respectively [68, 69]. According to our study, the presence of Ru 3d5/2 peaks was not observed. This could be due to the small loading of Ru species on the catalyst or the fact that the Ru species were highly covered by SiO_2 support. Moreover, the main peak of Ru was The O 1 s spectra of Ru/SiO_2 exhibited a strong signal centered at 534.5 eV, and these signals represent lattice oxygen [70,71]. The addition of Ti resulted in a shift of O1s peak to lower binding energies. The shift to lower binding energies of the O1s peak is probably due to the insertion of Ti in the SiO_2 matrix or the formation of Ru-O-Ti bonds. The Si 2p spectra of the Ru/SiO_2 exhibited the main peak at binding energies of 105 eV, which corresponds to Si^{4+} species in SiO_2 [72]. With the Ti doping, a shift in the position of the Si 2p peak towards lower binding energies was observed. This could result from increased silicon charge after doping with Ti [73], explaining the lower BE of the peak in these solids. Small XPS peaks of Ti 2p were also observed after adding Ti in FSP-made catalysts.

4.2. Catalytic test of FSP-made Ru/Ti-SiO_2 catalysts

The catalytic activity of all FSP-made catalysts was carried out in a CO_2 methanation reaction at temperatures between 200 and 400 °C. Fig. 4 shows the catalytic performance regarding CO_2 conversion as a function of reaction temperature. In all tests, there was no trace of CO formation. Among all catalysts, F-Ru-SiO_2 exhibited the lowest catalytic performance. Adding Ti improved catalytic performance, and F-Ru-12Ti-SiO_2 exhibited the highest CO_2 conversion. The better catalytic performance of Ti-doped catalysts could correlate to the presence of the TiO_2 phase, which increased Ru dispersion and created the interaction between Ti and Ru, which can be observed in XPS spectra. Moreover, the rutile phase prevents RuO_2 aggregation during calcination due to strong interactions between the RuO_2 and rutile-TiO_2 support, often facilitated by epitaxial matching [74,75]. In contrast, RuO_2 disperses poorly on anatase TiO_2, leading to sintering during calcination. Detailed studies on 5 wt% Ru supported on rutile TiO2 over a wide temperature range (200–800 °C) have shown minimal sintering of Ru nanoparticles, maintaining small particle sizes (2 to 3 nm) and high CO_2 methanation activity [76]. Rutile TiO_2, characterized by its tetragonal unit cell, can generate oxygen vacancies under reducing conditions, providing additional adsorption sites for CO_2 and thereby enhancing the CO_2 methanation reaction.

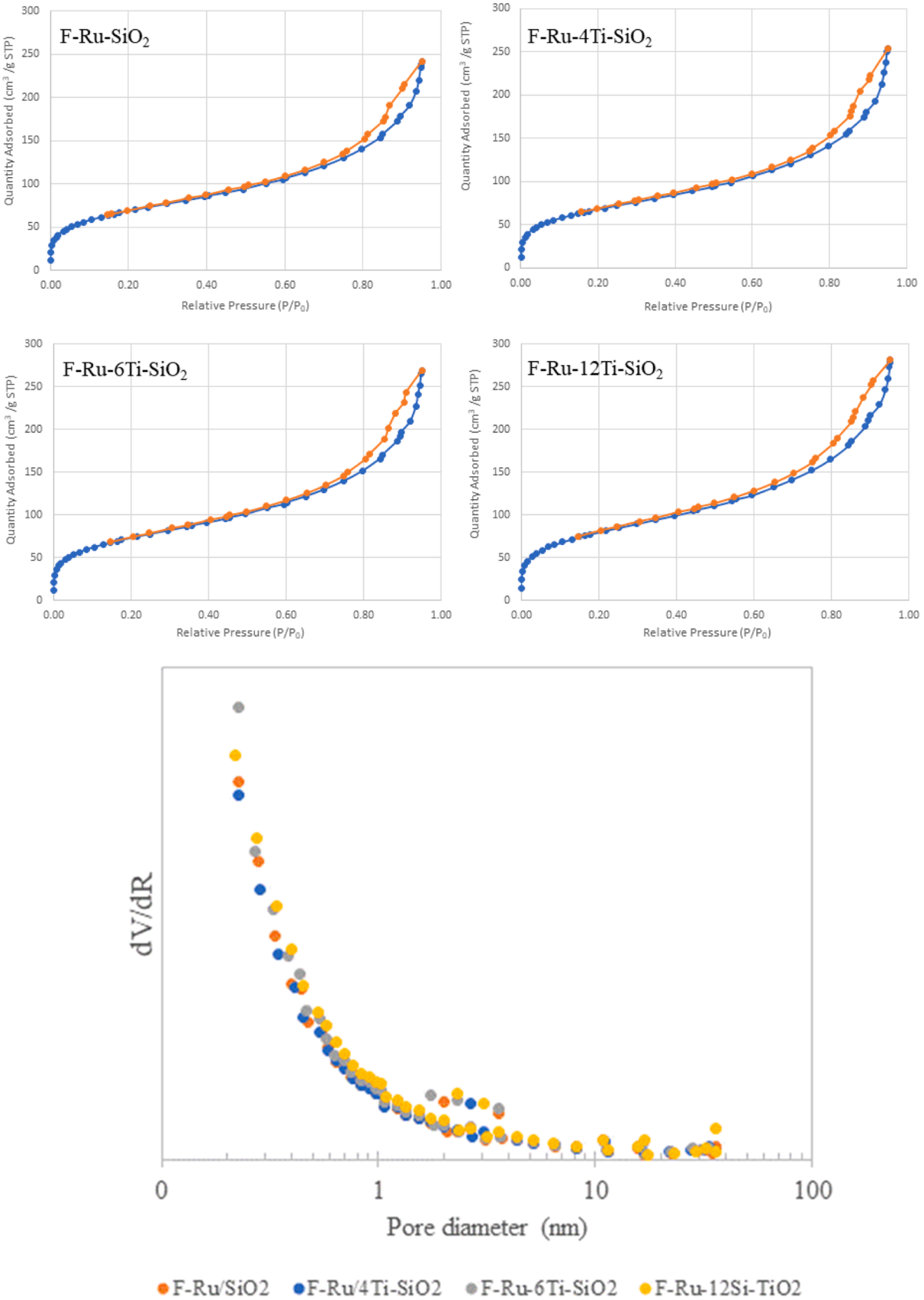


Fig. 2. The N_2 adsorption-desorption isotherms and pore size distribution of the FSP-made Ru/SiO_2 and $Ru/Ti\text{-}SiO_2$ catalysts.

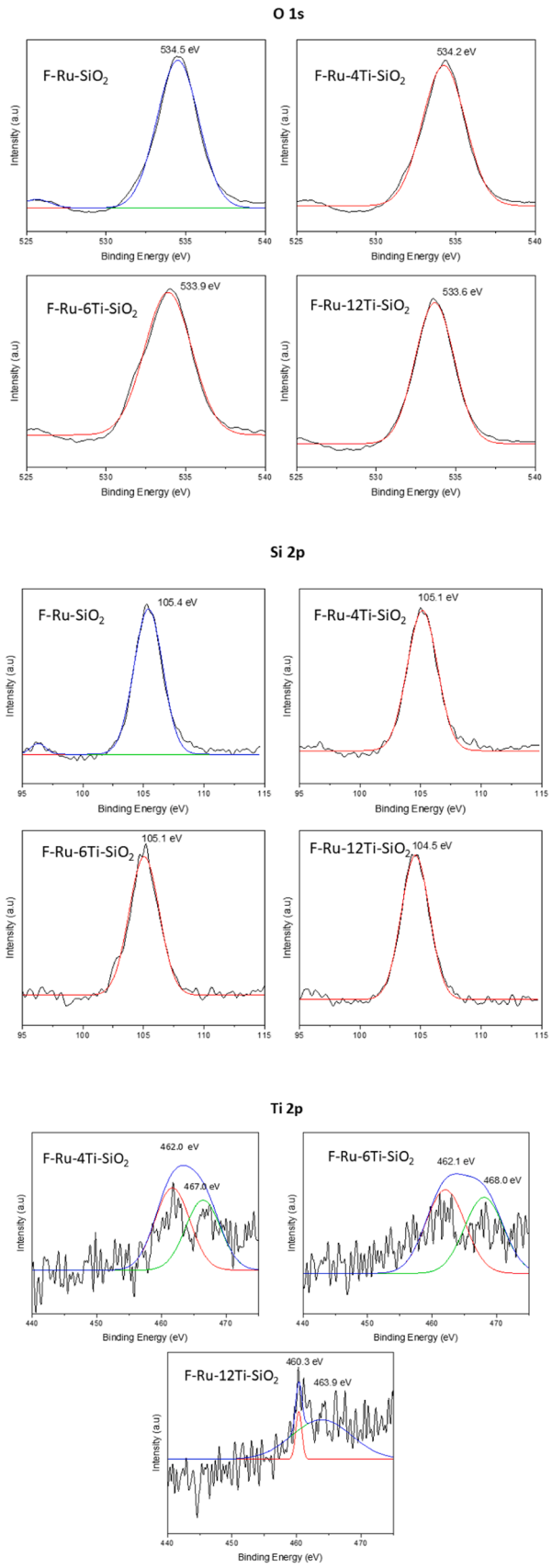


Fig. 3. XPS spectra of (a) O 1 s, (b) Si 2p, and (c)Ti 2p of FSP-made Ru/SiO_2 and Ru/Ti-SiO_2 catalysts.

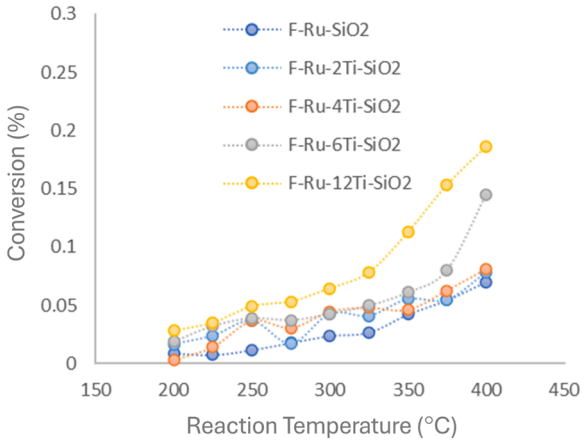


Fig. 4. The catalytic performance in terms of CO_2 conversion and reaction temperature of FSP-made Ru/SiO_2 and Ru/Ti-SiO_2 catalysts.

4.3. *Operando in-situ drifts study of catalysts*

To thoroughly understand the distinct mechanism and intermediate products of FSP-made Ru-supported catalysts, the *operando* and *in-situ* DRIFTS spectra of F-Ru-SiO_2 and F-Ru-12Ti-SiO_2 catalysts were measured under a continuous flow of the H_2/CO_2 gas at 200–400 °C. The obtained spectra are shown in Fig. 5. DRIFTS spectra of F-Ru-SiO_2 exhibited at 3735 - 3593 cm^{-1} are assigned to hydroxyl groups. After the reaction temperature increased to 300 °C, we found the presence of the characteristic bands at 2021 and 2125 cm^{-1} corresponding to the vibrational modes of CO adsorbed on metal Ru and adsorption of CO on ruthenium oxide surface [77]. The small characteristic band of CH_4 was observed at 3015 cm^{-1} after the temperature was raised to 400 °C. Similar characteristic bands were observed after adding 12wt% of Ti; however, the presence of both CO adsorption sites and the formation of CH_4 were already observed at lower temperatures. The CH_4 band was generated at 250 °C. The adsorption at lower temperatures might be the reason for higher catalytic activity after doping with Ti.

4.4. *Characterization of spent catalysts*

Fig. 6 shows the XRD profile of the spent of all FSP-made Ru supported on Ti-SiO_2 catalysts. The XRD profile of spent catalysts still exhibited the characteristic broad peaks of SiO_2 and the anatase and rutile phases of TiO_2. The RuO_2 peak is still present, with an additional peak at 2θ of 44° reflecting the existence formation of Ru metal. These results suggest that the RuO_2 phase on the FSP-made catalyst was partially reduced after the reaction. In addition, the XRD peak for TiO_2 phases had become narrower, which indicated the sintering of TiO_2 particles during the reaction test.

4.5. *Comparison results with impregnation-made catalysts*

To compare the catalytic performance of FSP-made catalyst, the Ru supported on Ti-modified SiO_2 catalysts have been synthesized via conventional impregnation of Ru on FSP-made Ti-SiO_2 support, and the obtained catalyst was also tested in CO_2 methanation reaction. A plot between CO_2 conversion and reaction temperature of FSP- (F-Ru-xTi-SiO_2) and impregnation-made (I-Ru/F-xTi-SiO_2) catalysts is shown in Fig. 7. It clearly shows that the catalyst prepared by the impregnation method exhibited much higher catalytic activities than FPS-made ones. Increasing Ti doping in SiO_2 support also improved the catalytic activity of Ru catalysts, and Ru/F-12Ti-SiO_2 exhibited the highest CO_2 conversion of 53 % at 40 °C.

Various characterization methods were applied to understand the higher catalytic activity of impregnation-made catalysts. XRD profiles of

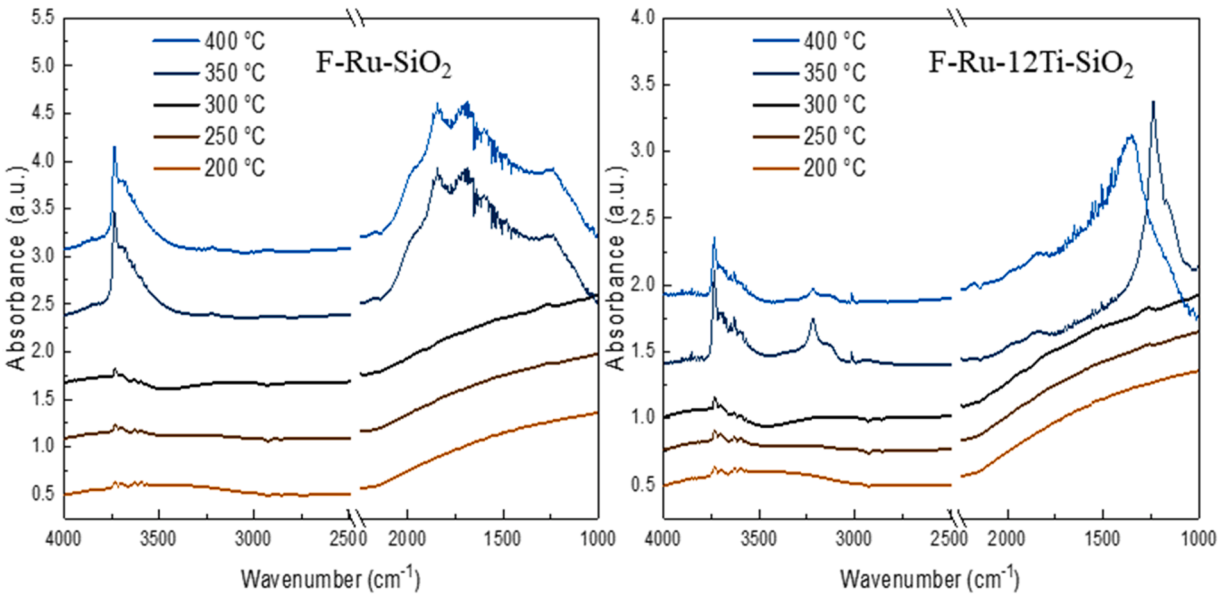


Fig. 5. Operando in-situ DRIFTS spectra of F-Ru-SiO_2 and F-Ru-12Ti-SiO_2 catalysts.

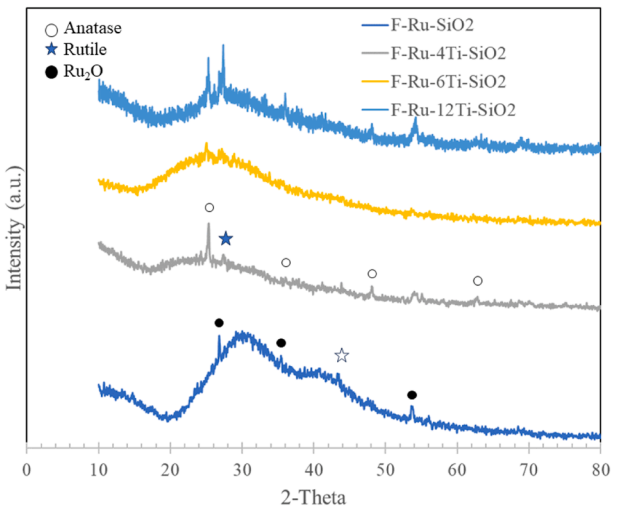


Fig. 6. XRD profile of spent FSP-made Ru/SiO_2 and Ru/Ti-SiO_2 catalysts.

the fresh FSP-made 12Ti-SiO_2 support, after impregnation and after catalytic testing are presented in Fig. 8. The XRD of pure support exhibited the broadband structure of amorphous silica with small peaks corresponding to anatase and rutile TiO_2 phases. After impregnation with Ru, the small peaks of RuO_2 were also observed. The crystal phases of the fresh impregnation catalyst were quite similar to the catalyst made by one-pot FSP. However, after the reaction test, RuO_2 peaks in the fresh catalysts sample were completely absent, and the additional peaks of Ru metal were present. This suggested that the RuO_2 on the impregnation-made catalyst was completely transformed into a Ru metallic phase after the reaction. This phenomenon is quite different from the FSP-made catalysts, in which only the partial reduction of the RuO_2 phase is presented after the reaction. Thus, this might be the reason for the observed high catalytic performance of impregnation-made catalysts.

Other physical properties such as BET surface area, total pore volume, crystallite size, and active sites of impregnation catalyst are summarized in Table 2. BET surface area and total pore volume of impregnation-made catalyst ranged around 91.7 to 163.8 m^2/g and 0.55 to 1.43 cm^3/g, respectively. The surface area of impregnation-made catalysts was much lower than that of FSP-made catalysts, and the increase of Ti doping decreased both surface area and pore volume. The

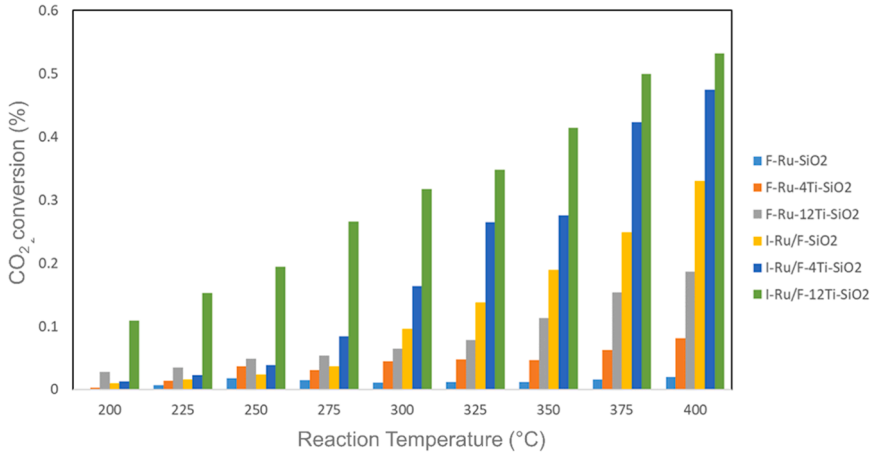


Fig. 7. The graph between CO_2 conversion and reaction temperature of FSP- and impregnation-made Ru/SiO_2 and Ru/Ti-SiO_2 catalysts.

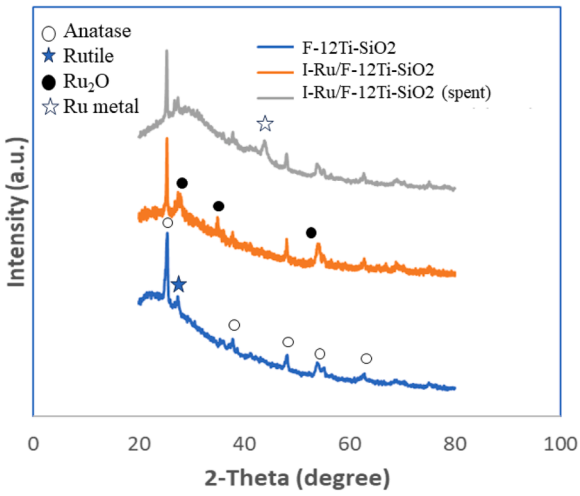


Fig. 8. XRD profile of FSP-made 12Ti-SiO_2 support, after impregnation and after catalytic test.

Table 2
The physiochemical of all impregnation-made catalysts.

Catalyst	BET surface areas (m^2/g)	Pore Volume (cm^3/g)	d_{XRD} (nm)[a]	Active site (μmol/g-cat)	Dispersion (%)
I-Ru/F-SiO_2	163.8	1.43	–	2.4	4.6
I-Ru/F-4 %Ti-SiO_2	137.2	0.74	23.6	7.4	14.4
I-Ru/F-12 %Ti-SiO_2	91.7	0.55	25.4	7.6	15.1

[a] Calculated by using the Scherrer equation from anatase peak at $2\theta = 25$.

lower surface area of impregnation-made catalysts probably came from the calcination process after impregnation, which causes the interparticle void collapse and particle sintering. However, the pore volume of impregnation-made catalysts was higher than that of FSP-made catalysts. This result suggests that adding Ru in the flame reactor, together with Ti and Si precursors, resulted in a huge decrease in pore volume. This is probably due to the trapping of RuO_2 molecules inside the pore structure of support, which makes it hard for H_2 molecules to diffuse to reduce the RuO_2 crystal and leave it partially reduced after the reaction. The coverage of SiO_2 over metal particles has been reported in our previous works regarding the FSP-made Pd/SiO_2 catalysts for 1-heptyne hydrogenation [24]. The FSP-made catalysts exhibited a very low amount of active site due to the coverage of SiO_2 on Pd particles, which prohibited H_2 adsorption on the Pd surface. The formation of catalysts by flame synthesis occurs in the gas phase. The metal precursors fed in the flame reactor were combusted and released the metal atom, which was crystallized, agglomerated, and aggregated to form the products. In this case, Ru_2O, with a lower boiling point, would crystallize first, and then it would be covered by TiO_2 and SiO_2.

The CO_2 methanation mechanism and intermediate products of impregnation-made Ru-supported catalysts are also studied using the operando in-situ DRIFTS methods, and the results are shown in Fig. 9. The characteristic bands of CO adsorbed on metal Ru at 2021 cm^{-1} were found at 200 °C, and the band of CO adsorbed on ruthenium oxide – expected at 2125 cm^{-1} – was not detected. An additional band at 1580 cm^{-1} was present. This band corresponds to the formation of formate (*HCOO) species, which generally decomposes to *CO and finally hydrogenates to CH_4. The characteristic band of CH_4 was also found at the same temperature, which suggested that the CH_4 might be produced via

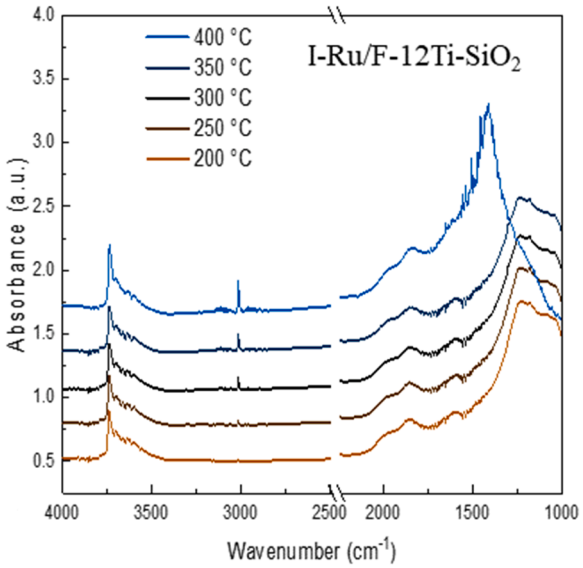


Fig. 9. Operando in-situ DRIFTS spectra of I-Ru/F-12Ti-SiO_2 catalysts.

the formate route. In many literature reports, the methanation reaction can occur by two main routes. First, the formation of CO intermediate (*CO) via formate species at the Ru–support interface (formate route):

$$CO_2 + H^* \rightarrow {}^*HCOO \rightarrow {}^*CO + {}^*OH.$$

Another possible mechanism is the dissociative adsorption of CO_2 to the *CO intermediate (CO route):

$$CO_2 \rightarrow {}^*CO + {}^*O$$

The operando results clearly show that the addition of Ti promotes the catalytic activity of Ru-supported SiO_2 catalysts, and impregnation-made catalysts exhibit higher catalytic activity than FSP-made ones. In the case of FSP-made catalysts, the formation of CH_4 would occur through the CO route, while the impregnation-made catalysts might proceed via dissociative adsorption of CO_2 and the formation of surface formats. Different catalytic routes might be used to explain the difference in catalytic activity of both catalysts.

4.6. DFT calculation

To further study the effect of Ti loading on Ru/SiO_2 catalysts, Ru adsorption energy, Ru-bandgap, and CO_2 adsorption energy were determined by using the first-principles density functional theory (DFT) calculation [39–42] to reveal the effects of Ti doping on the performance of Ru/SiO2 catalysts. The interaction between the Ru metal and the supports was analyzed through the adsorption energy (E_{ads}) of Ru on anatase TiO_2 (A-TiO_2), SiO_2, and Ti-SiO_2 supports, where the stable geometry of Ru on various supports will be derived based on the energy minimization of each system, as shown in Fig. 10. Among them, the interaction between Ru and A-TiO_2 is the strongest, as reflected through the most negative E_{ads} at −4.96 eV, while the interaction between Ru and the SiO_2 support is the weakest. Interestingly, the addition of Ti onto the SiO_2 support was found to enhance the adsorption strength of Ru on the support; in other words, it can be implied that the using of less expensive support of SiO_2 modified with a small amount of Ti may improve the performance of the catalyst comparable to the anatase TiO_2. Also, it can indicate that the addition of Ti on SiO_2 significantly enhances the stability of the Ru support catalyst against leaching.

Moreover, the density of states (DOS) calculation was carried out to realize the electronic properties of the catalyst system together with the derivation of the bandgap of the support of Ru catalysts. The addition of Ru was found to reduce the bandgap for all three supports, as shown in

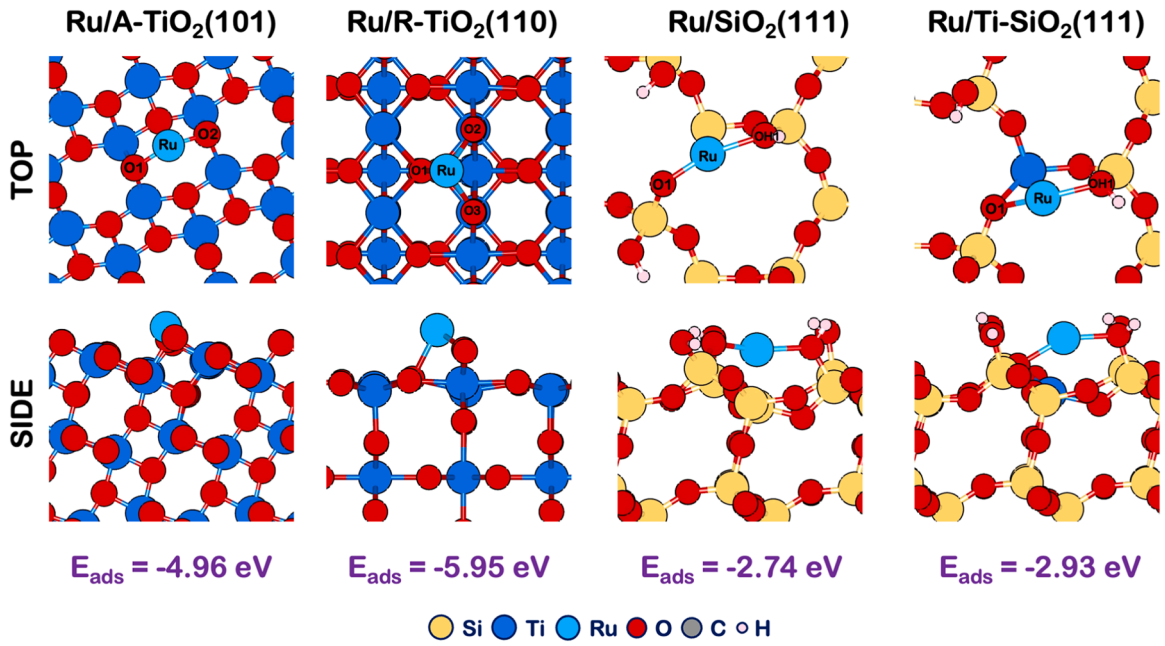


Fig. 10. Fig. 1 The adsorption energy of Ru on A-TiO_2, R-TiO_2, SiO_2, and Ti-SiO_2 support.

Fig. 11, indicating the improvement in the performance of the Ru catalyst. Interestingly, the Ru/Ti-SiO_2 catalyst exhibited the lowest band gap at 1.00 eV compared to the Ru/A-TiO2 and Ru/SiO2 catalyst exhibiting band gap at 2.82 and 2.20 eV, respectively. In addition, the Bader charge analysis and charge density differences have revealed that the electron donation came from the Ru atom to the A-TiO_2 at +1.12 |e|, indicating the strong interaction between support and Ru that is also confirmed by the highest adsorption energy of Ru on A-TiO_2 support.

Thereafter, to investigate the catalytic performance of the Ru catalysts, the adsorption of CO_2 on all systems, that all possibilities of CO_2 adsorption in each system are elucidated in the SI, is performed to observe the strength of CO_2 binding on the catalyst surface during the reaction. As can be seen in Fig. 12, the adsorption energy of CO_2 was in the order of Ru/Ti-SiO_2 (−1.27 eV) > Ru/R-TiO_2 (−1.11 eV) > Ru/SiO_2 (−0.60 eV) > Ru/A-TiO_2 (−0.56 eV), where the more negative the value, the stronger the adsorption of CO_2. This indicates the stronger binding of CO_2 on the Ti-modified SiO_2 Ru catalyst compared to other catalysts.

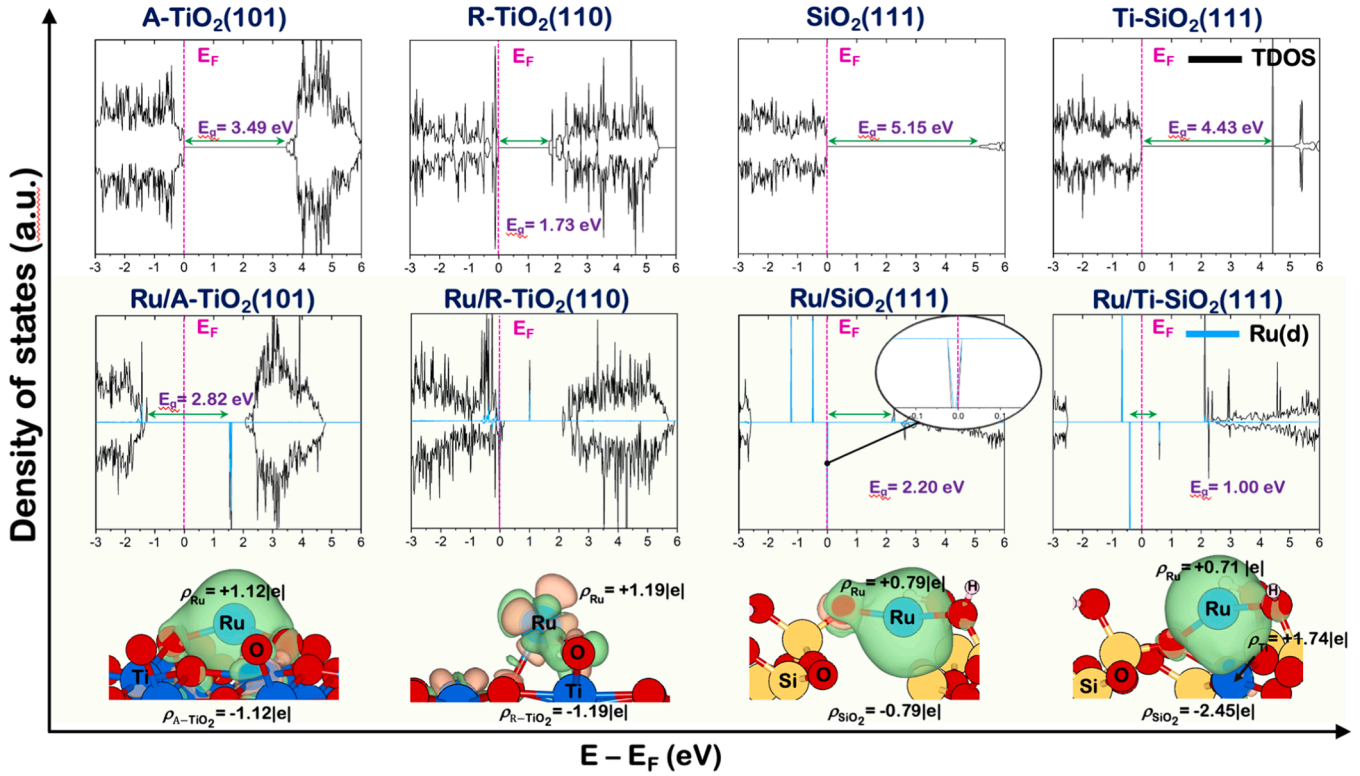


Fig. 11. The band gap and charge transfer between support and Ru on catalysts of undoped support, Ru/A-TiO_2, Ru/R-TiO_2, Ru/SiO_2, and Ru/Ti-SiO_2 catalyst.

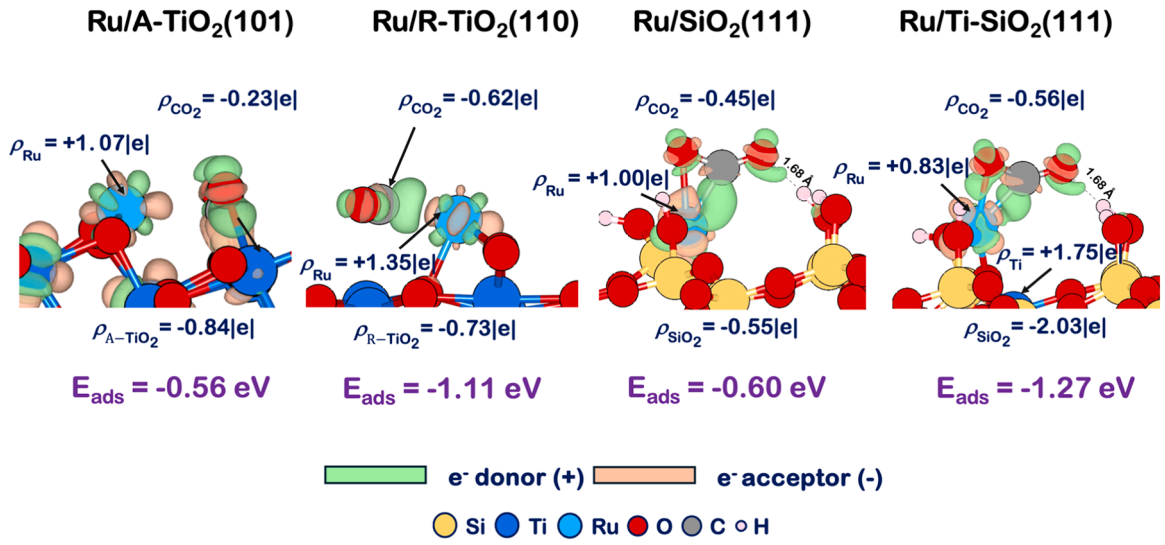


Fig. 12. The adsorption energy of CO_2 and charge transfer between catalysts and molecule of CO_2 on Ru/A-TiO_2, Ru/R-TiO_2, Ru/SiO_2, and Ru/Ti-SiO_2 catalyst.

Furthermore, the Bader charge analysis and charge density differences were performed again on this CO2-adsorbed catalyst system to analyze the charge transfer between the catalyst and the molecule of CO_2 on the catalyst. The charge donation from Ru/Ti-SiO_2 to the CO_2 molecule at −0.56 |e| was found to be higher than that of the Ru/A-TiO_2 (−0.23 |e|) and Ru/SiO_2 (−0.45 |e|) as displayed in Fig. 13, which indicates a strong interaction between the catalyst and CO_2 molecule during the reaction, confirmed by the most negative adsorption energy found on Ru/Ti-SiO_2.

The performance of the SiO_2-supported catalyst is evaluated by considering the enthalpy of the reaction for CO_2 dissociation, as shown in Fig. 13. It was found that the endothermic reaction was observed on Ru/SiO_2 at +1.39 eV (+134.11 kJ/mol), while the exothermic reaction was observed on Ru/Ti-SiO_2, with the heat of reaction at - 0.25 eV (−24.12 kJ/mol).

5. Conclusions

Ru supported on SiO_2 and Ti-SiO_2 catalysts have successfully been prepared in one step by using flame spray pyrolysis. The addition of Ti resulted in the formation of anatase and rutile TiO_2 mixed in the catalyst particles. Increasing Ti loading improved the catalytic activity in CO_2 methanation. The presence of the TiO_2 phase promotes the catalytic activity by increasing Ru dispersion and retard the RuO_2 sintering during the high-temperature process, which according to the strong interaction between RuO_2 and rutile-TiO_2. However, the catalytic activity of FSP-made catalysts is much lower than that of impregnation-made ones. From in-situ IR Drift spectra results, the CH_4 formation mechanism of both catalysts was different. In the case of FSP-made catalysts, the formation of CH_4 might probably occur through the CO route, while the impregnation-made catalysts may proceed via dissociative adsorption of CO_2 and the formation of surface formate. The difference in the CH_4 methanation mechanism might be due to the different stages of Ru species in the reaction process. The DFT advocates that doping with Ti

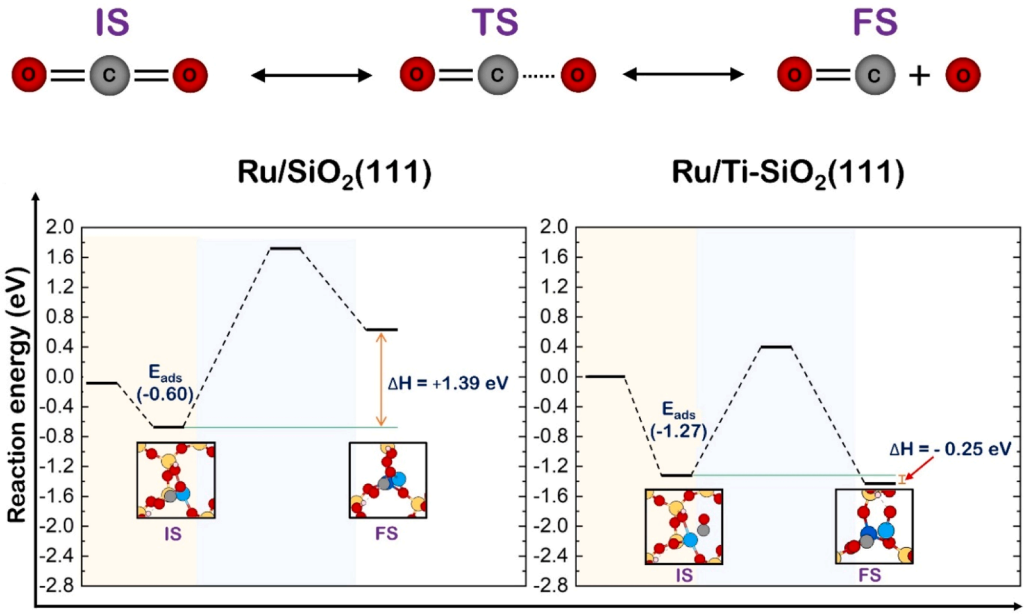


Fig. 13. The comparison between reaction energy for CO_2 dissociation on Ru/SiO_2 and Ru/Ti-SiO_2 catalyst.

increases the interaction between Ru and support and decreases the band gap of the system, which then promotes the catalytic activity of the catalyst.

CRediT authorship contribution statement

Okorn Mekasuwandumrong: Writing – review & editing, Writing – original draft, Visualization, Validation, Methodology, Investigation, Formal analysis, Data curation, Conceptualization. **Tinnakorn Saelee:** Writing – review & editing, Supervision, Investigation. **Jakapob Noppakhun:** Writing – review & editing, Writing – original draft, Visualization, Validation, Investigation. **Meena Rittiruam:** Writing – review & editing, Validation. **Patcharaporn Khajondetchairit:** Writing – review & editing, Validation. **Damien P. Debecker:** Writing – review & editing, Validation, Supervision, Project administration, Formal analysis, Conceptualization. **Supareak Praserthdam:** Writing – review & editing, Writing – original draft, Visualization, Validation, Supervision, Software, Resources, Project administration, Methodology, Investigation, Funding acquisition, Formal analysis, Conceptualization. **Piyasan Praserthdam:** Writing – review & editing, Supervision, Project administration, Investigation, Conceptualization.

Declaration of competing interest

The authors declare that they have no known competing financial interests or personal relationships that could have appeared to influence the work reported in this paper.

Acknowledgments

The research has received funding support from (1) NSRF via the Program Management Unit for Human Resource & Institutional Development, Research and Innovation [grant number B1640034], (2) the Second Century Fund (C2F), Chulalongkorn University, (3) Mid-Career Research Grant 2024 (N42A670295), the National Research Council of Thailand (NRCT), and (4) Thailand Science Research and Innovation Fund Chulalongkorn University (IND_FF_68_054_2100_009). All computational resources are supported by the high-performance computing unit (CECCHCU) at Chulalongkorn University, Thailand. Lastly, we would like to acknowledge Prof. Wasu Chaitree reconstruction and analysis of the revised XPS spectra.

Supplementary materials

Supplementary material associated with this article can be found, in the online version, at doi:10.1016/j.mcat.2025.115179.

Data availability

Data will be made available on request.

References

[1] M.M. Faruque Hasan, L.M. Rossi, D.P. Debecker, K.C. Leonard, Z. Li, B.C. E. Makhubela, C. Zhao, A. Kleij, ACS Sustainable Chem. Eng. 9 (2021) 12427–12430.
[2] W. Wei, G. Jinlong, Front. Chem. Sci. Eng. 5 (1) (2010) 2–10.
[3] B. Miao, S.S.K. Ma, X. Wang, H. Su, S.H. Chan, Catal. Sci. Tech. 6 (2016) 4048–4058.
[4] M.A.A. Aziz, A.A. Jalil, S. Triwahyono, A. Ahmad, Green. Chem. 17 (2015) 2647–2663.
[5] K. Müller, M. Städter, F. Rachow, D. Hoffmannbeck, D. Schmeißer, Environ. Earth. Sci. 70 (2013) 3771–3778.
[6] A. Behr, Chem. Eng. Technol. 10 (1987) 16–27.
[7] S. Carenco, C. Sassoye, M. Faustini, P. Eloy, D.P. Debecker, H. Bluhm, M. Salmeron, J. Phys. Chem. C 120 (2016) 15354–15361.
[8] J. Martins, N. Batail, S. Silva, S. Rafik-Clement, A. Karelovic, D.P. Debecker, A. Chaumonnot, D. Uzio, Catal. Commun. 58 (2015) 11–15.
[9] H.H. Shin, L. Lu, Z. Yang, C.J. Kiely, S. McIntosh, ACS. Catal. 6 (5) (2016) 2811–2818.
[10] Y. Zhao, V. Girelli, O. Ersen, D.P. Debecker, J. Catal. 426 (2023) 283–293.
[11] M. Agnelli, M. Kolb, C. Mirodatos, J. Catal. 148 (1994) 9–21.
[12] M. Agnelli, H. Swaan, C. Marquez-Alvarez, G. Martin, C. Mirodatos, J. Catal. 175 (1998) 117–128.
[13] D.C. Upham, A.R. Derk, S. Sharma, H. Metiu, E.W. McFarland, Catal. Sci. Technol. 5 (2015) 1783–1791.
[14] J. Xu, X. Su, H. Duan, B. Hou, Q. Lin, X. Liu, X. Pan, G. Pei, H. Geng, Y. Huang, J. Catal. 333 (2016) 227–237.
[15] G. Garbarino, D. Bellotti, P. Riani, L. Magistri, G. Busca, Int. J. Hydrogen Energ. 40 (2015) 9171–9182.
[16] C. Janke, M.S. Duyar, M. Hoskins, R. Farrauto, Appl. Catal., B 152-153 (2014) 184–191.
[17] A.H. Zamani, R. Ali, W.A. Bakar, J. Taiwan. Inst. Chem. Eng. 45 (2014) 143–152.
[18] C. Li, S. Zhang, B. Zhang, D. Su, S. He, Y. Zhao, J. Liu, F. Wang, M. Wei, D.G. Evans, X. Duan, J. Mater. Chem. A 1 (2013) 2461.
[19] A.M. Abdel-Mageed, D. Widmann, S.E. Olesen, I. Chorkendorff, J. Biskupek, R. J. Behm, ACS. Catal. 5 (2015) 6753–6763.
[20] A. Kim, D. P.Debecker, F. Devred, V. Dubois, C. Sanchez, C. Sassoye, Appl. Catal. B 220 (2018) 615–625.
[21] L. Mädler, W.J. Stark, S.E. Pratsinis, J. Mater. Res. 18 (2003) 115–120.
[22] O. Mekasuwandumrong, S. Somboonthanakij, P. Praserthdam, J. Panpranot, Ind. Eng. Chem. Res. 48 (2009) 2819–2825.
[23] O. Mekasuwandumrong, S. Somboonthanakij, P. Praserthdam, J. Panpranot, Ind. Eng. Chem. Res. 48 (2009) 2819–2825.
[24] O. Mekasuwandumrong, S. Phothakwanpracha, B. Jongsomjit, A. Shotipruk, J. Panpranot, Catal. Lett. 136 (2010) 164–170.
[25] P. Pawinrat, O. Mekasuwandumrong, J. Panpranot, Catal. Commun. 10 (2009) 1380–1385.
[26] I. Rossetti, L. Fabbrini, N. Ballarini, C. Oliva, F. Cavani, A. Cericola, B. Bonelli, M. Piumetti, E. Garrone, H. Dyrbeck, E.A. Blekkan, L. Forni, J. Catal. 256 (2008) 45–61.
[27] D.P. Debecker, B. Schimmoeller, M. Stoyanova, C. Poleunis, P. Bertrand, U. Rodemerck, E.M. Gaigneaux, J. Catal. 277 (2011) 154–163.
[28] W. Kohn, L.J. Sham, Phys. Rev. 140 (1965) A1133.
[29] G. Kresse, J. Non-Cryst. Solids 192 (1995) 222–229.
[30] G. Kresse, J. Furthmüller, Phys. Rev. B 54 (1996) 11169.
[31] G. Kresse, J. Furthmüller, Comput. Mater. Sci. 6 (1996) 15–50.
[32] G. Kresse, J. Hafner, Phys. Rev. B 49 (1994) 14251.
[33] P.E. Blöchl, Phys. Rev. B 50 (1994) 17953.
[34] G. Kresse, D. Joubert, Phys. Rev. B 59 (1999) 1758.
[35] J.P. Perdew, K. Burke, M. Ernzerhof, Phys. Rev. Lett. 77 (18) (1996) 3865.
[36] M. Methfessel, A. Paxton, Phys. Rev. B 40 (6) (1989) 3616.
[37] H.J. Monkhorst, J.D. Pack, Phys. Rev. B 13 (12) (1976) 5188.
[38] N.A. Deskins, M. Dupuis, Phys. Rev. B 75 (2007) 195212.
[39] M.E. Arroyo-de Dompablo, A. Morales-García, M. Taravillo, J. Chem. Phys. (2011) 135.
[40] G. Mattioli, F. Filippone, P. Alippi, A.Amore Bonapasta, Phys. Rev. B 78 (2008) 241201.
[41] Z. Cheng, T. Liu, C. Yang, H. Gan, F. Zhang, J. Chen, J. Phys. Chem. Solids 73 (2012) 302–307.
[42] M.H. Samat, A.M.M. Ali, M.F.M. Taib, O.H. Hassan, M.Z.A. Yahya, Results. Phys. 6 (2016) 891–896.
[43] S.M. Rasul, D.R. Saber, S.B. Aziz, Results. Phys. 38 (2022) 105688.
[44] N.A. Deskins, M. Dupuis, Phys. Rev. B 75 (2007) 195212.
[45] M.E. Arroyo-de Dompablo, A. Morales-García, M. Taravillo, J. Chem. Phys. (2011) 135.
[46] S. Grimme, J. Antony, S. Ehrlich, H. Krieg, J. Chem. Phys. 132 (15) (2010).
[47] V. Finkel, X-ray diffraction study of the thermal expansion of Ru, Os and re at 77-300 K, Phys. Met. Metallogr. 32 (1) (1971) 231–235.
[48] R.W.G. Wyckoff, A survey of existing crystal structures data, JB Lippincott (1923).
[49] M. Černohorský, The ratio method for absolute measurements of lattice parameters with cylindrical cameras, Acta Crystallogr. 13 (10) (1960) 823–826.
[50] Y. Urashima, T. Wakabayashi, T. Masaki, Y. Terasaki, Ruthenium, a new mineral from Horokanai, Hokkaido, Japan, Mineralog. J. 7 (5) (1974) 438–444.
[51] R. Ross, W. Hume-Rothery, High temperature X-ray metallography: I. A new debye-scherrer camera for use at very high temperatures II. A new parafocusing camera III. Applications to the study of chromium, hafnium, molybdenum, rhodium, ruthenium and tungsten, J. Less Common Metals 5 (3) (1963) 258–270.
[52] A. Morozkin, Y.D. Seropegin, Sm–Ru–Ge system at 1070 K, J. Alloys. Compd. 365 (1–2) (2004) 168–172.
[53] O. Mohan, S. Shambhawi, R. Xu, A.A. Lapkin, S.H. Mushrif, ChemCatChem. 13 (2021) 2420–2433.
[54] H.-Y. Ma, G.-C. Wang, J. Phys. Chem. C 125 (2021) 18161–18169.
[55] H.-Y. Ma, G.-C. Wang, Appl. Surf. Sci. 603 (2022) 154398.
[56] A. Vittadini, A. Selloni, F.P. Rotzinger, M. Grätzel, Phys. Rev. Lett. 81 (14) (1998) 2954.
[57] V. Shklover, et al., Chem. Mater. 9 (2) (1997) 430–439.
[58] S.J. Moniz, S.A. Shevlin, X. An, Z.X. Guo, J. Tang, Chemistry–Eur. J. 20 (47) (2014) 15571–15579.
[59] X.-Q. Gong, A. Selloni, M. Batzill, U. Diebold, Nat. Mater. 5 (8) (2006) 665–670.
[60] U. Diebold, N. Ruzycki, G.S. Herman, A. Selloni, Catal. Today 85 (2–4) (2003) 93–100.
[61] H.-L.T. Le, J. Goniakowski, C. Noguera, A. Koltsov, J.-M. Mataigne, Phys. Chem. Chem. Phys. 20 (9) (2018) 6254–6263.
[62] X. Rozanska, F. Delbecq, P. Sautet, Phys. Chem. Chem. Phys. 12 (45) (2010) 14930–14940.

[63] C. Li, X. Yang, Y. Guo, Mater. Sci. Semicond. Process. 150 (2022) 106964.
[64] M. Zhang, M. Gao, J. Chen, Y. Yu, RSC. Adv. 5 (33) (2015) 25959–25966.
[65] I.-S. Chuang, G.E. Maciel, J. Phys. Chem. B 101 (16) (1997) 3052–3064.
[66] J. Yang, S. Meng, L. Xu, E. Wang, Phys. Rev. B 71 (3) (2005) 035413.
[67] A. Swapnesh, V.C. Srivastava, I.D. Mall, Chem. Eng. Technol. 37 (2014) 1765–1777.
[68] K. Qadir, S.M. Kim, H. Seo, B.S. Mun, F. A.Akgul, Z. Liu, J.Y. Park, J. Phys. Chem. C 117 (2013) 13108–13113.
[69] K.S. Kim, N. Winograd, J. Catal. 35 (1947) 66–72.
[70] M. Li, L. Zeng, Y. Chen, L. Zhuang, X. Wang, H. Shen, Int. J. Photoenergy 2013 (2013) 352473.
[71] D.S. Jensen, S.S. Kanyal, N. Madaan, Surf. Sci. Spectra 20 (2013) 36–42, 1.
[72] S.P. Chenakin, G. Melaet, R. Szukiewicz, N. Kruse, J. Catal. 312 (2014) 1–11.
[73] J. Cañón, A.V. Teplyakov, Surf. Interf. Anal. 53 (2021) 475–481.
[74] F. Wang, C. Li, X. Zhang, M. Wei, D.G. Evans, X. Duan, J. Catal. 329 (2015) 177–186.
[75] A. Kim, C. Sanchez, G. Patriarche, O. Ersen, S. Moldovan, A. Wisnet, C. Sassoye, D. P. Debecker, Catal. Sci. Technol. 22 (2016) 8117–8128.
[76] A. Swapnesh, V.C. Srivastava, I.D. Mall, Chem. Eng. Technol. 37 (2014) 1765–1777.
[77] B. Miao, S.S.K. Ma, X. Wang, H. Su, S.H. Chan, Catal. Sci. Technol. 6 (2016) 4048–4058.